A DISCRETE APPROACH FOR PREDICTING VOID FORMATION DURING VACUUM CONSOLIDATION OF AUTOCLAVE COMPOSITES

Guillaume Seon, Andrew Makeev, Yuri Nikishkov, Brian Shonkwiler
University of Texas at Arlington
Arlington, TX, USA

ABSTRACT

Porosity/voids are common manufacturing defects in laminated composite components and structures. The susceptibility to manufacturing defects greatly increases in contoured autoclave composite sections. In particular, composite helicopter rotor components are typically thick and often have areas with a tight radius of curvature, which make them especially prone to process-induced porosity defects. Tight radii inherently result in non-uniform consolidation pressure, causing the formation of large voids, or pockets of entrapped air, at ply interface. Such defects may significantly affect structural integrity and increase rejection rates in the production of rotor composite components. Recent advances in high-fidelity non-destructive inspection of composites, such as X-ray Computed Tomography (CT), have shown that reduction of strength and fatigue performance of laminates can be strongly related to shape, size, and location of individual critical voids at ply interface. However, none of the existing tools available for process modelling are able to predict the formation of such individual defects, including their geometry and position in the composite parts.

The Office of Naval Research (ONR) project "Physics-Based Composite Process Simulation" seeks to fill the gaps in understanding the underlying physical principles governing the formation and evolution of manufacturing defects. In particular, understanding and modelling defect formation at the early stages of the manufacturing process might be the missing link to enable the development of practical engineering solutions allowing for better control of the manufacturing process. Debulking, or vacuum consolidation, has been a common practice extensively used by rotorcraft manufacturers to reduce the amount of "bulk" or air entrapped during the lay-up of curved and thick composite rotor components prior to curing. The debulking process typically spans several hours and requires intensive manual interventions. Yet, parameters controlling the debulking process, including frequency, temperature and pressure, are determined empirically with no guaranty that they are optimum or applicable when new materials and new geometries are introduced.

This work presents the latest developments of a new approach introduced by the authors that relies on finite element modeling (FEM) and discrete representation of the critical entrapped air pockets at ply interface for simulation of air removal during vacuum consolidation of autoclave prepreg composites. The approach uses cohesive elements enriched with pore pressure degree of freedom inserted at ply interface. In particular, this work includes the development of an experimental procedure for measurement of the cohesive properties associated with the tackiness of uncured autoclave prepregs. Experimental results are also compared with FEM simulation for validation of the discrete modeling approach.

Copyright 2019. Used by the Society of the Advancement of Material and Process Engineering with permission.

SAMPE Conference Proceedings. Charlotte, NC, May 20-23, 2019. Society for the Advancement of Material and Process Engineering – North America.

1. INTRODUCTION

Porosity/voids are common manufacturing defects in laminated composite components and structures. Recent advances in high-fidelity non-destructive inspection of composites, such as X-ray Computed Tomography (CT), have shown that reduction of strength and fatigue performance of laminates can be strongly related to shape, size, and location of individual critical voids at ply interface [1-3]. However, none of the existing tools available for process modelling are able to predict the formation of such individual defects, including their geometry and position in the composite parts.

X-Ray CT data of uncured laminates after manual layup and prior to autoclave curing reveal multiple large pockets of entrapped air at ply interface, suggesting that understanding defect formation at the early stages of the manufacturing process might be the missing link to enable the development of practical engineering tools enabling mitigation of the manufacturing defects [4]. Air is easily entrapped during the layup process due to the tackiness of the pliable prepreg material, which might be regarded as a pressure-sensitive adhesive material, coupled with the fact that air permeability of typical raw thermoset prepreg plies used in autoclave manufacturing is very low, at least prior to resin flow. Low air permeability is the result of full saturation of the fiber reinforcement with the liquid thermoset resin during the fabrication of autoclave prepregs. The ability of air pockets to migrate and be removed from the laminate during the debulking process is likely to be strongly local and dependent on many factors, including initial distribution of entrapped air, presence and geometry of air pathways, proximity to laminate edges, pressure gradients and other factors that might modify the local tackiness at ply interface.

It is worth noting that homogenized air extraction models based on Darcy's Law and representation of the prepreg material as a porous material have been used by researchers to predict air evacuation in partially impregnated panels used in out-of-autoclave manufacturing [5,6]. Partial impregnation of out-of-autoclave composites results in high cross-sectional area for air flow through multiple channels or air pathways distributed within the center of each ply of the prepreg material. In this situation, homogenization of the prepreg material as a bi- or tri-phases porous medium might be applicable. In fully-impregnated autoclave prepregs, in the other hand, pockets of entrapped air prior to consolidation represent discontinuities within the laminate which cannot be ignored.

In Ref. [4], the authors introduced a new numerical approach based on the explicit modeling of the discontinuities associated with critical voids in autoclave prepregs. This approach relies on the use of cohesive elements enriched with pore pressure degree of freedom for discrete representation of the pockets of entrapped air at ply interface. The pore pressure cohesive zone approach has been originally developed for geomechanics problems [7-9]. In Ref. [4], the authors demonstrated applicability of the method to composite manufacturing using a benchmark problem where entrapped air at ply interface in a flat laminate is removed by application of a rigid tool.

In this work, which is part of an effort that seeks to fill the gaps in understanding the underlying physical principles governing the formation and evolution of manufacturing defects, the development of an experimental procedure for measurement of the cohesive properties associated with the tackiness of uncured autoclave prepregs is presented. Uncured carbon/epoxy prepregs might act as pressure-sensitive adhesives with the ability to instantly form a bond when brought into contact with a surface, without requiring heat or chemical treatment. The cohesive strength and dissipation energy required to separate the bonded tacky surfaces might be influenced by numerous factors including dwell force, dwell time, pulling rate, surface cleanliness and environmental conditions. It is expected that tackiness plays an important role in the formation of defects during vacuum consolidation of contoured polymer-matrix composite laminates.

Preliminary measurements of the tackiness properties of uncured IM7/8552 prepreg material are presented in this work. Experimental data is also compared with numerical results for validation of the discrete modeling approach.

2. DISCRETE APPROACH

2.1 Pore-Pressure Cohesive Zone Modeling

The diagram in Figure 1 illustrates the discrete modeling concept for an air pocket entrapped at the interface between two impermeable layers of tacky material. As shown in Figure 1, an air-filled pocket is represented by a fully broken cohesive zone where transverse fluid flow and air injection is permitted. At air pocket boundaries, the cohesive zone is partially broken and surface tractions are nonzero due to tackiness of the interface between the two media, which resists the reaction forces due to distribution of air pressure.

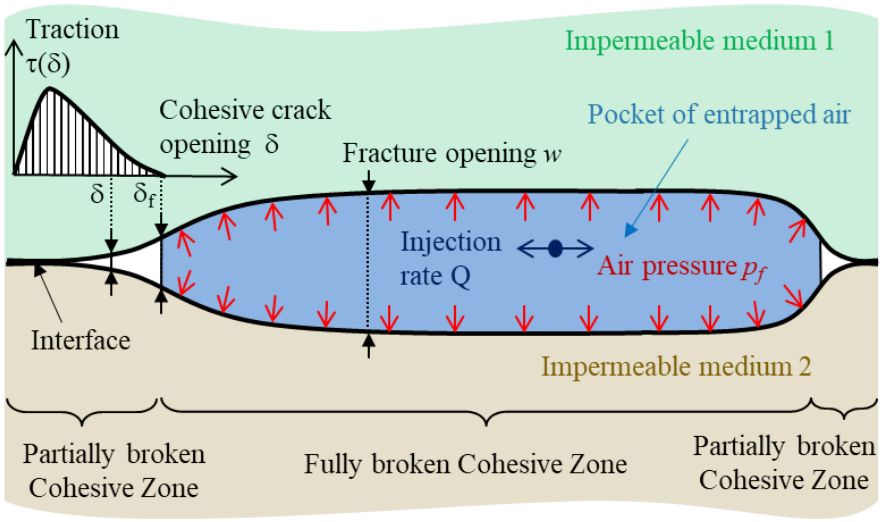


Figure 1. Pore pressure cohesive zone modelling for an air pocket entrapped at the interface between two impermeable media.

The relationships between the deformation of the surrounding material, the pressure p_f inside the pocket of entrapped air and the cohesive law representing the bonding and debonding process at the interface is found by solving a system of coupled constitutive equations which are summarized below for reference. The reader might refer to Refs. [7-9] for more background and recent developments on the derivation and implementation of the constitutive equations with applications to fluid-driven fracture problems in rock mechanics.

Assuming that the air entrapped between the two layers of material behaves as an incompressible fluid with Newtonian rheology, the tangential flow within the broken cohesive zone is governed by the equation of mass conservation:

$$\frac{\partial w}{\partial t} + \nabla . \boldsymbol{q} = Q(t)\delta(\boldsymbol{x}, \boldsymbol{x}_0) \quad [1]$$

where $\boldsymbol{q}$ is the fluid flux of the tangential flow, w is the fracture opening, Q is the fluid injection rate and $\delta(\boldsymbol{x}, \boldsymbol{x}_0)$ is a spatial Dirac function equal to unity at the point of fluid injection.

The flux of tangential flow $\boldsymbol{q}$ can be related to the gradient of fluid pressure ∇p_f along the cohesive zone according to the Poiseuille's law:

$$\boldsymbol{q}w = -k_t \nabla p_f \quad [2]$$

where k_t is the tangential permeability to air flow, which might be defined as a function of the gap opening w according to Reynold's equation:

$$k_t = \frac{w^3}{12\mu} \quad [3]$$

with μ the fluid viscosity.

Continuity of displacement on the crack faces imposes:

$$w = \boldsymbol{u}.\boldsymbol{n} \quad [4]$$

Where $\boldsymbol{u}$ is the displacement field in the surrounding material and $\boldsymbol{n}$ is the local unit normal vector to the crack faces.

The fracture process at the crack tip is modelled using a traction-separation law that relates the effective traction tensor $\boldsymbol{\tau'}$ to the separation $\boldsymbol{\delta}$ across the cohesive surfaces:

$$\boldsymbol{\tau}' = \frac{\partial \phi}{\partial \delta} \quad [5]$$

ϕ is a cohesive potential function that describes the bonding and debonding process at the interface between the two layers of surrounding material, including description of the tacky behavior.

The effective cohesive tractions can be related to the stress tensor $\boldsymbol{\sigma}$ in the surrounding material from the system of equations resulting from force equilibrium at the crack faces:

$$\boldsymbol{\sigma}.\boldsymbol{n}^+ = -\boldsymbol{\sigma}.\boldsymbol{n}^- = \boldsymbol{\tau}' - p_f \boldsymbol{n} \quad [6]$$

Deformation in the surrounding media is described by their respective mechanical constitutive relations. For an air pocket entrapped between two layers of the same material, only one set of constitutive equations is needed. In the framework of an anisotropic hyper-elastic material, the constitutive relation might be defined by relating the Cauchy stress tensor $\boldsymbol{\sigma}$ to a strain energy potential function $\boldsymbol{\psi}$ and the hydrostratic pressure p [10]:

$$\boldsymbol{\sigma} = \frac{2}{J}\boldsymbol{F}\frac{\partial \boldsymbol{\psi}}{\partial \boldsymbol{C}}\boldsymbol{F}^T - p\boldsymbol{I} \quad [7]$$

where $\boldsymbol{F}$ is the deformation gradient, $\boldsymbol{C}$ is the right Cauchy-Green deformation tensor such as $\boldsymbol{C} = \boldsymbol{F}.\boldsymbol{F}^T$, $J = \det(\boldsymbol{F})$ and $\boldsymbol{I}$ is the second-order identity tensor.

Finally, the tress tensor $\boldsymbol{\sigma}$ is also related to the deformation of the material and the applied body forces $\boldsymbol{b}$ through the equation of conservation of momentum:

$$\nabla.\boldsymbol{\sigma} + \rho\boldsymbol{b} - \rho\ddot{\boldsymbol{u}} = 0 \quad [8]$$

Where ρ is the density of the material and $\ddot{\boldsymbol{u}}$ is the acceleration vector.

2.2 Implementation

The constitutive model described in the previous section is implemented in Abaqus/Standard FE solver for the simulation of entrapped air at the interface between plies of uncured prepreg material. The uncured prepreg is assumed to be fully resin-saturated and impermeable to air flow in the out-of-plane direction. Such assumptions are representative of the behavior of uncured autoclave carbon/epoxy prepregs during vacuum consolidation or debulking. Implementation of the model is summarized in this section. The reader might also refer to [4] for additional details. The Abaqus/Standard coupled pore fluid flow and stress analysis solver for transient analysis is used to solve the set of coupled constitutive equations (1-8) in a weak form in the time domain [11].

2.2.1 Cohesive Constitutive Behavior

The pore-pressure cohesive model is implemented using zero-thickness cohesive pore pressure elements available in the Abaqus/Standard element library [11]. In this work, 12-nodes 3D pore pressure cohesive elements COH3D3P are used. A 12-node COH3D3P element is illustrated in Figure 2. As shown in Figure 2, the element includes eight nodes with displacement and pore pressure degree of freedom and four additional pore pressure nodes defined in the gap interior.

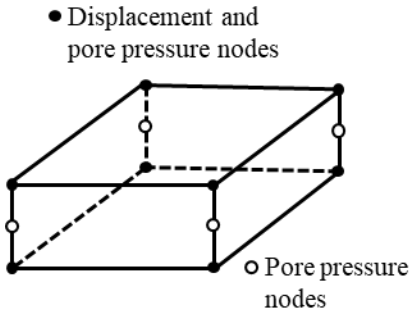


Figure 2. Twelve-node COH3D3P elements available in Abaqus/Standard.

The cohesive traction-separation law used in this work is implemented within an Abaqus/Standard User Material subroutine UMAT. The cohesive model is based on the mixed-mode bilinear traction-separation laws introduced by Turon et al for simulation of interlaminar delamination failure in composites under mixed-mode loading [12]. It is worth noting that Turon et al bi-linear traction-separation cohesive model is available in Abaqus/Standard built-in material models. However, the available built-in models for definition of P-CZM properties do not allow for the modelling of tackiness.

The tackiness, or pressure sensitive behavior, is included in the cohesive constitutive model by the introduction of a history state variable (SDV1) within the UMAT subroutine. The state variable is set to unity when a previously open cohesive element is closed under compressive loading and set to zero when a previously closed element is re-opened. The state variable is used within UMAT to fully restore the cohesive properties of broken cohesive elements that undergo compressive loading. The state variable is also passed to user subroutine USDFLD to assign solution dependent properties to the tangential air flow permeability k_t and prevent tangential flow in cohesive elements under compressive loading until further tensile loading occurs.

The flowchart diagram for the update of history state variable SDV1 and the interactions between the UMAT subroutine, USDFLD subroutine and Abaqus/Standard pore fluid flow and analysis solver is summarized in Figure 3.

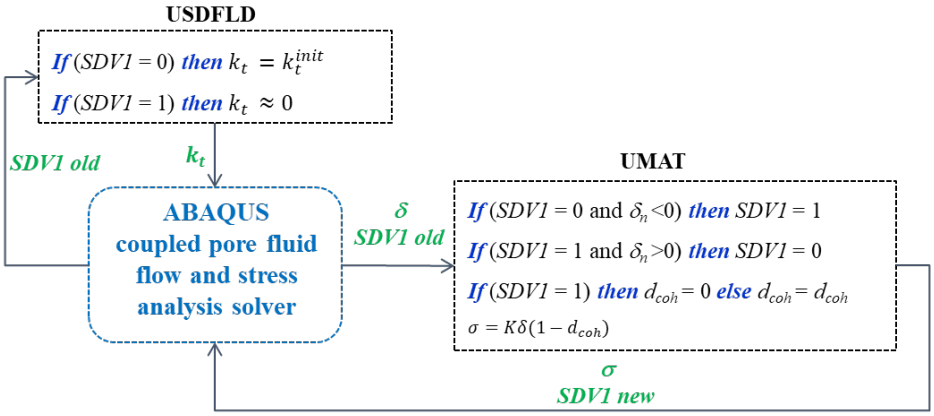


Figure 3. Flowchart for implementation of the effects of tackiness.

2.2.2 Bulk Material Constitutive Behavior

The constitutive model used to describe the mechanical response of the uncured prepreg material is based on a hyperelastic transverse isotropic constitutive model proposed in [13] for modeling soft-matrix fiber-reinforced materials. This model uses a Neo-Hookean type of strain energy potential function $\boldsymbol{\psi}$ defined by four constants and the four strain invariants I_1, J, I_4 and I_5:

$$\boldsymbol{\psi} = \frac{\mu}{2}(I_1 - 3) - \mu ln(J) + \frac{\lambda}{2}(J-1)^2 + [\alpha + \beta ln(J) + \gamma(I_4 - 1)](I_4 - 1) - \frac{\alpha}{2}(I_5 - 1) \quad [9]$$

One advantage of the Neo-Hookean model above is that the four constitutive properties α, β, λ, and μ can be related to the material constants in a transverse isotropic Hooke's laws type of constitutive relationships that should be valid at small strains [13]. Hooke's law and associated engineering material constants are easily interpreted since they can be related to standard mechanical tests. The relationships between α, β, λ, and μ and small strains engineering material constants E_f, E_m, ν and G is given in Ref. [13]. E_f, Em, ν and G refer to the Young's modulus in the fiber direction, Young's modulus in the matrix direction, in-plane Poisson's ratio and in-plane shear modulus, respectively. The constitutive model defined by equations (7) and (9) is implemented in Abaqus/Standard user subroutine UANISOHYPER_INV.

3. AIR FRACTURE TESTING

3.1 Concept

An air fracture test setup was developed in this work with the objectives to improve our understanding of the physics involved in the debulking process of uncured prepreg materials and allow measurement of key material characteristics, including measurement of tackiness properties. The concept for the air fracture test setup is illustrated in Figure 4.

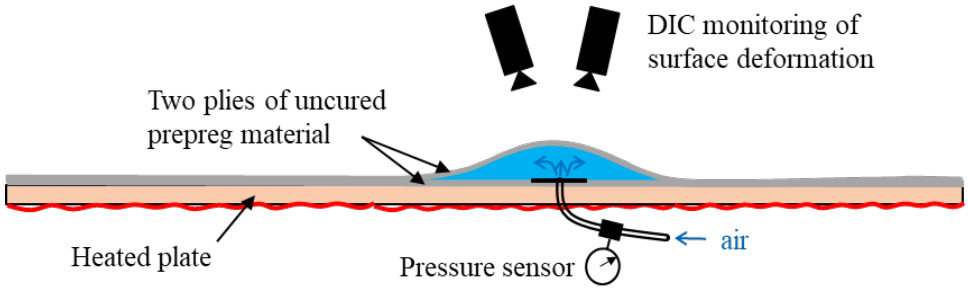


Figure 4. Air fracture test concept.

As shown is Figure 4, the idea of the air fracture test is to inject air at the interface between two plies of uncured prepreg materials that are bonded together due to tackiness. The prepreg material is fully resin-saturated and can be considered impermeable to out-of-plane air flow. As air is injected between the two impermeable plies, air-driven fracture is expected to occur with debonding of the tacky interface and the formation of a pocket of entrapped air.
Surface deformation, including the out-of-plane displacement related to the cohesive gap opening between the two plies, can be monitored using a stereo Digital Image Correlation (DIC) system. Air pressure within the air pocket can be monitored using a pressure sensor placed on the tube at air intake. Under-quasi static conditions, the pressure at the air intake should be equal to the pressure within the air pocket. Also, the cohesive tractions at the interface should balance the air pressure within the entrapped air pocket. Therefore, the cohesive traction-separation properties could be inferred from simultaneous measurement of air pressure and out-of-plane displacement. It is assumed that the air-driven debonding process is mode I dominated, which is a reasonable assumption that can be verified by comparing out-of-plane with in-plane displacements in the full-field 3D DIC data.
Prior to testing, the two plies of prepreg can be bonded together using a weight placed on the surface of the top ply and the influence of dwell time and dwell force can be studied to characterize the pressure sensitive behavior. As illustrated in Figure 4, the bottom ply of prepreg material can also be laid on a heated plate to study the effect of temperature on tackiness and pore-pressure cohesive properties.

3.2 Development of a Test Setup

General views of the test setup developed in this work according to the test concept introduced in Figure 4 are shown in Figures 5a and 5b. Detailed views of the test specimen bottom and top plies and bottom ply installed in the test fixture are provided in Figures 6a and 6b.

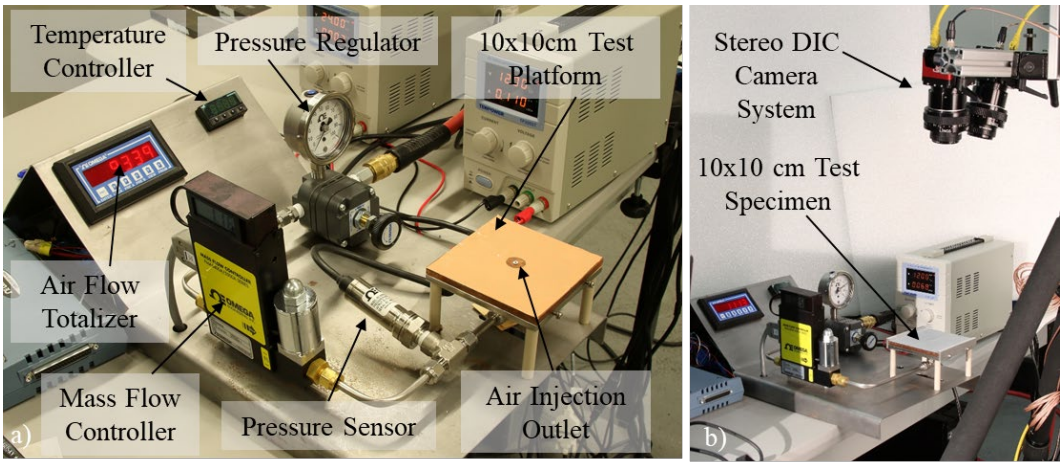


Figure 5. a) General view of the test setup and b) setup with stereo DIC camera system.

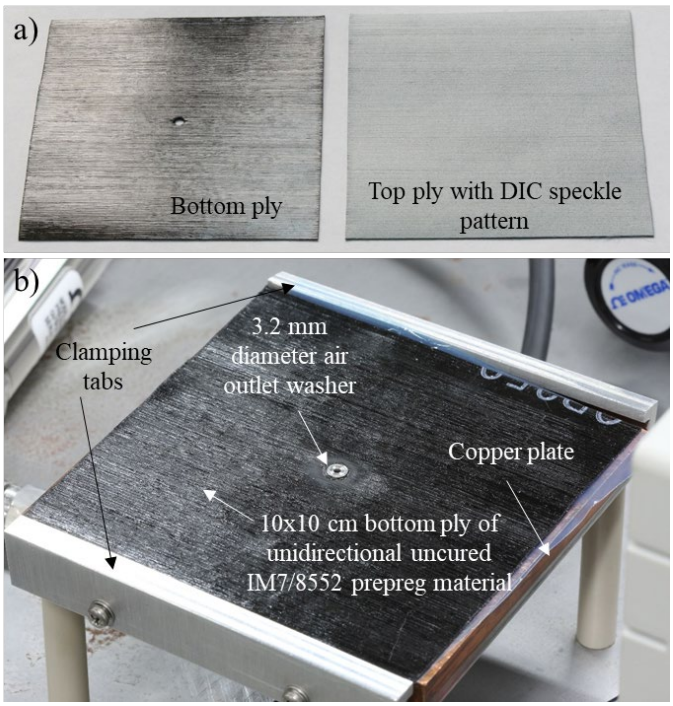


Figure 6. a) 10x10 cm bottom and top plies of raw prepreg material used in the air fracture test and b) bottom ply installed on the test platform.

As shown in Figure 5a, the test setup includes a temperature controller, air flow totalizer, mass flow controller, pressure sensor and a test platform designed to hold 10x10 cm test specimens. A 3.2 mm hole is punched on the bottom ply to allow the air injection post to pass through as illustrated in Figure 6a. The bottom ply is placed on the test platform, which includes a copper plate that can be heated for elevated temperature testing. A random speckle pattern is created using black and white spray paints on the surface of the top ply for DIC measurement of surface deformation. Two of the specimen edges can be clamped under clamping tabs, as shown in Figure 6b.

4. TEST RESULTS

4.1 Test Configurations

Air fracture testing was accomplished using uncured 10x10 cm square pieces of uncured IM7/8552 prepreg material. The two unidirectional plies of were stacked up such as their respective fiber direction is aligned along the same direction and tests were conducted at room temperature. Prior to testing, a 9kg weight was placed on the top surface of the laminate and left for 15 minutes to ensure bonding of the two tacky ply interfaces. Air was injected at a constant rate of 2ml per minute. Two configurations A and B were tested.

In configuration A, the two opposite edges of the specimen along the fiber direction were clamped in the test fixture and no Teflon insert was used to pre-debond the interface on top of the air injection outlet. In configuration B, all specimen edges were left free and a 16 mm diameter circular piece of Teflon film was positioned on top of the air injection washer to prevent bonding during application of the 9kg weight. Configurations A and B are illustrated in Figure 7.

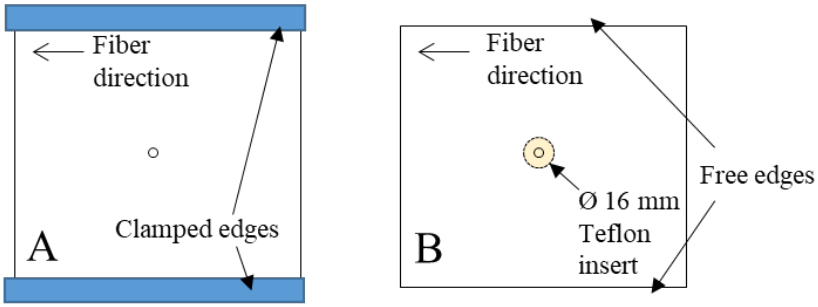


Figure 7. Two configurations A & B of air fracture specimens tested.

4.2 Test Results for Configuration A

Figure 8 shows contours plots of the DIC-measured out-of-plane surface displacement at different times during air fracture testing of a specimen tested in Configuration A. As air is injected at the center of the laminate, a pocket of entrapped air is formed at the interface between the two plies. The maximum out-of-plane deflection for the air pocket after 150s was about 1.5 mm. Pressure information was not available in this experiment.

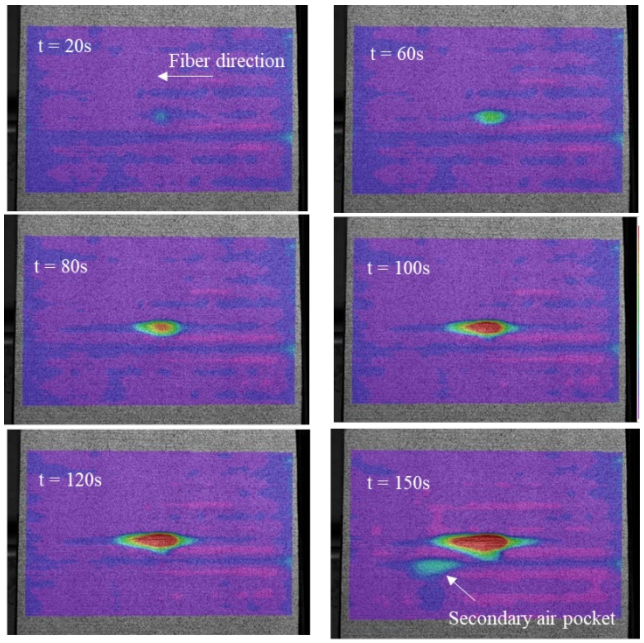


Figure 8. Contour plots of the DIC-measured out-of-plane surface displacement at different times during air fracture testing of a specimen in Configuration A

As illustrated in Figure 8, progression of air fracture is anisotropic with a preferred direction of propagation along the fiber direction. It is worth noting that similar elongated "noodle" shapes oriented along the fiber direction are typically observed for the critical voids observed at ply interface in cured laminates. This observation consolidates the assumption that the void geometry might be determined at the very early stage of the manufacturing process, during the layup and debulking operations and prior to curing.

Figure 8 also shows the formation of a secondary air pocket after the main pocket has reached a certain size. Test data suggests that this pocket is formed due to air seepage through open or weakened channels at the interface between the plies bonded together due to tackiness. This phenomenon will be part of further investigations.

4.3 Test Results for Configuration B

Similar to Figure 8, Figure 9 shows DIC contour plots of out-of-plane surface displacement measured at different times during air injection in test Configuration B. As shown in Figure 9, the air pocket formed during air injection is less elongated than for Configuration A, which can be attributed to the presence of a circular Teflon insert in Configuration B. However, directionality of the debonding process along the fiber direction becomes evident once air fracture progresses beyond the initial debonded area.

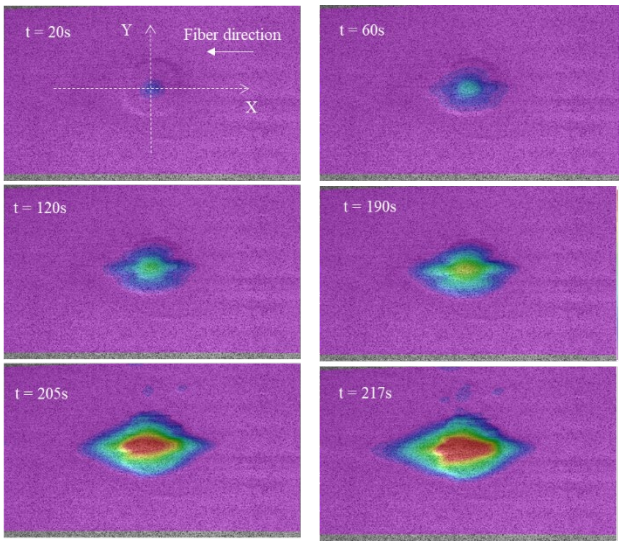


Figure 9. DIC out-of-plane displacement in test Configuration B.

Figures 10a and 10b show time history profiles for the out-of-plane deflection along the X axis indicated in Figure 9 and the evolution of air pressure with time, respectively. Pressure was measured in test Configuration B using a pressure sensor located between the air injection outlet and the air mass flow controller, as shown in Figure 5a (this measure was not available in test Configuration A, unfortunately).

As illustrated in Figure 10, two regimes can be identified. In Regime 1, the pressure and the maximum deflection are increasing almost linearly with time. During this regime, the spatial extension of the air pocket along the X axis is relatively limited and constant. This regime corresponds to the air filling, or inflation, of the pre-debonded interfacial area covered by the circular Teflon insert. The correlation between increase in air pressure and increase of the deflection suggests near quasi-static conditions during this regime. The peak pressure is reached at the end of Regime 1 around 200s, which is followed by rapid decrease in air pressure and rapid increase in maximum deflection with propagation of the debonding along the X axis. This regime is a transient regime corresponding to the rapid propagation of air-driven fracture at the interface.

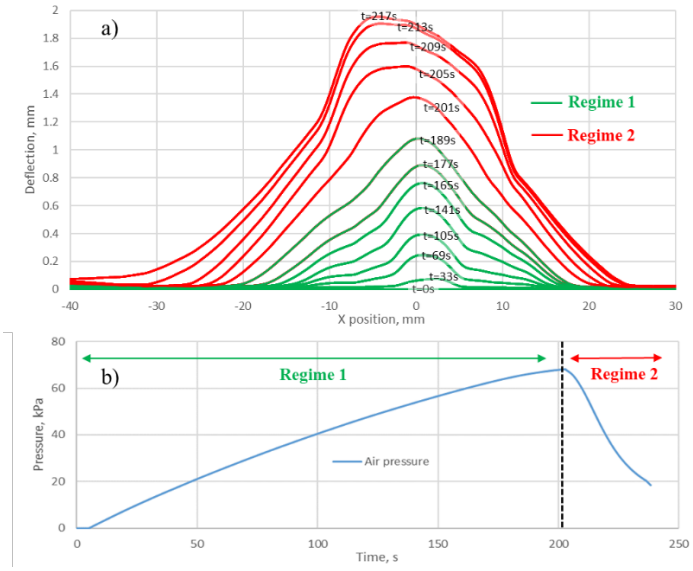


Figure 10. a) Time history deflection profiles and b) evolution of air pressure.

The abovementioned considerations support the assumption that the peak pressure corresponds to the initiation of debonding for a prepreg interface that has been optimally bonded at room temperature under the 9kg pressure force applied prior to testing. Therefore, the 68 kPa peak pressure is a measure of the interply cohesive strength of IM7/8552 uncured prepreg material, or tackiness, under these conditions.
Measurement of the cohesive strength as a function of the dwelling force, dwelling time and temperature will be part of the future work.

5. VALIDATION OF THE MODELING APPROACH

5.1 FE Model

Figure 11 shows an example of a 3D finite element mesh representative of the air fracture test in Configuration A presented previously. A layer of 3D zero-thickness pore-pressure cohesive elements COH3D8P is inserted between the two plies of prepreg material. In this model, cohesive elements share nodes with the surrounding C3D8 solid elements used to model the bulk material. One element per ply thickness is used in the bulk layers, which have a thickness of 0.394 mm corresponding to the uncured ply thickness of the IM7/8552 prepreg that was used in air fracture testing.

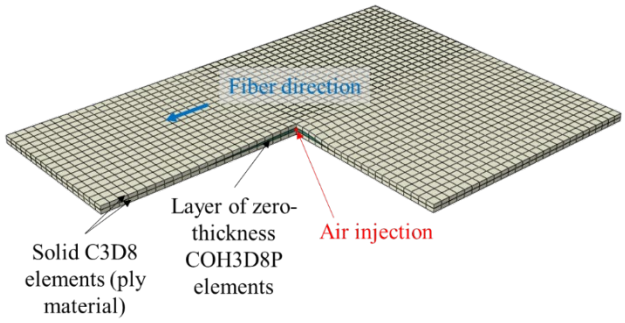


Figure 11. 3D finite element mesh representative of the air fracture test in Configuration A.

Air injection is simulated by prescribing a node-based flow loading condition (CFLOW) at the pore-pressure node located in the center of the laminate in the pore-pressure cohesive layer. An injection rate of 2ml/min is used to reproduce the air fracture testing conditions described in the previous section. The hyperelastic transverse isotropic constitutive model described in Section 2.2.2 is used for the material of the bulk layers. The four constant α, β, λ, and μ are calculated from the engineering material constants E_f, E_m, ν and G as defined in Ref. [13]. In this preliminary model, a modulus of 827 MPa is used for the Young's modulus E_m in the transverse direction. This corresponds to the debulked compaction modulus measured by the authors in previous work for uncured IM7/8552 prepreg [4]. Poisson's ratio and shear Modulus ν and G, respectively, are estimated based on the considerations presented in Ref. [4]. The Young's modulus in the fiber direction E_f is calculated from different values of the ratio R of the longitudinal modulus over the transverse modulus $R = E_f/E_m$.

A bilinear cohesive law is used for description of the mechanical response of the pore-pressure cohesive layer, as described in Section 2. The 68 kPa mode I cohesive strength measured in the air fracking test in Configuration B for IM7/8552 prepreg is used. The debonding process is assumed to be mode I dominated. The rest of the pore-pressure cohesive properties used in the model, including the initial linear stiffness, mode I fracture toughness, pore fluid viscosity and initial gap opening are selected in this preliminary work based on consistency of the length scale, time scale and force magnitudes involved. Further characterization will be part of future work.

5.2 FE Simulation Results

Figure 12 shows the progression of the air fracture process in a FE model representative of the air fracture test in Configuration A, where air is injected at the center of the laminate at constant flow rate. In these results, the ratio R of the longitudinal modulus over the transverse modulus is equal to 100. For visualization purpose, the deformation scale has been multiplied by 4. The maximum out-of-plane deflection at 100% of simulation time is about 0.3 mm.

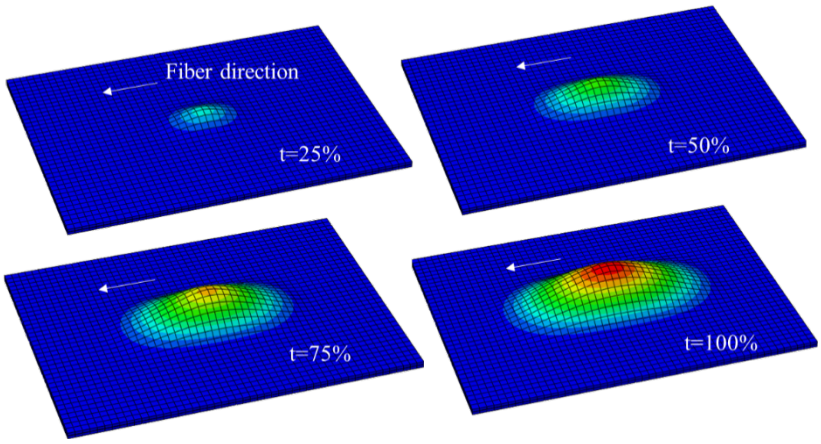


Figure 12. Progression air fracture in FE model representative of test Configuration A

As illustrated in Figure 12, progression of air fracture is not isotropic. A pocket of entrapped air develops into an elongated shape, with a preferred direction of propagation along the fiber direction. The isotropic progression of air fracture is a consequence of the isotropic constitutive response of the prepreg material and coupling between the air fracture process with the deformation of the surrounding ply material. At the debonding front, the pore pressure is balanced by the cohesive tractions and the far-field stress. At slow injection rates, pore pressure is more or less uniform within the air pocket. Bending in the longitudinal fiber direction is limited due to the high tensile/compressive modulus of the fibers; therefore, cohesive forces quickly increase to compensate the increase of air pressure for a crack front progressing in the fiber direction. On the other hand, transverse modulus of the prepreg material is very low and the increase in pressure can be absorbed by large transverse bending. Large transverse bending "slows down" the progression of the debonding front in the transverse direction.
This effect is further illustrated in Figure 13, where out-of-plane displacement contour plots show the final progression of the debonding front for different *R* ratio values.

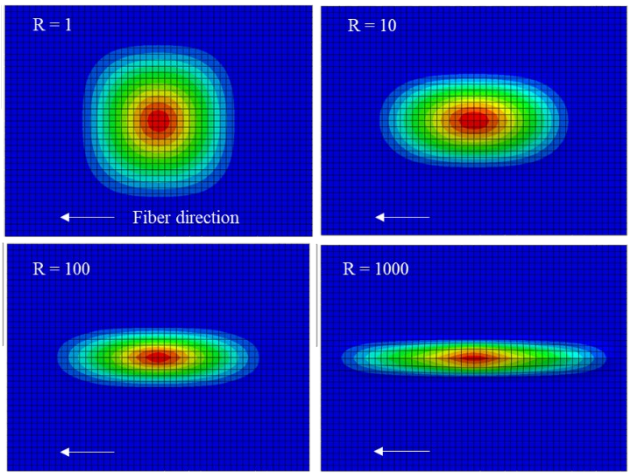


Figure 13. Final progression of debonding and out-of-plane displacement at different *R* ratio values.

As illustrated in Figure 13, air fracture progresses in isotropic fashion when the longitudinal modulus of the material is equal to its transverse modulus ($R = 1$). For a high ratio $R = 1000$, progression of air fracture is strongly directional, with the pocket of entrapped air developing into a "noodle-like" shape oriented along the fiber direction. These qualitative results correlate very well with the progression of air fracture observed in test and shown in Figures 8 and 9. This demonstrates the ability of the discrete pore-pressure cohesive approach to capture the physics involved in the formation of critical voids in autoclave prepreg laminates.
It is worth noting that the progression of air fracture observed during testing, and shown in Figures 8-10, is not perfectly uniform nor symmetrical, as opposed to the simulation results presented in Figures 12&13. This discrepancy highlights the complexity of the physics involved in air transport and vacuum consolidation in autoclave composites. In particular, the local ply interface tackiness and susceptibility to entrapped air migration might be influenced by many factors, such as non-uniform pressure application during layup, prepreg waviness, surface cleanliness and other sources of non-uniformity that are not accounted for in the simulation. Future work will evaluate

repeatability of the experiments and the impact of non-uniformities on predictability and accuracy of the numerical model.

6. CONCLUDING REMARKS

Developing the composite process simulation tools capable of predicting critical defects, including voids at ply interfaces, and integrating them with available tools for structural diagnostics and performance prediction are essential for closing the loop on effective control of the manufacturing process to prevent formation of critical defects in autoclave composite parts. In this work, we presented the latest developments of a new approach based on discrete modelling of the critical entrapped air pockets at ply interface for simulation of air removal during debulking of autoclave prepreg composites. In particular, we demonstrated both experimental and numerical evidence that the geometry of critical voids at ply interfaces in autoclave composites, which typically have a "noodle shape" oriented along the fiber direction, might be determined at the very early stage of the manufacturing process. We also showed that tackiness of the raw material and the process of air fracture at ply interface is likely to play a significant role in the formation of critical voids and presented preliminary measurements of the tackiness of uncured IM7/8552 prepreg material.

7. ACKNOWLEDGMENTS

This research was partially funded by the U.S. Office of Naval Research under Grant N00014-18-1-2120. Such support is gratefully acknowledged. The views and conclusions contained in this document are those of the authors and should not be interpreted as representing the official policies, either expressed or implied, of the U.S. Government. The authors also thank Mr. Ed Lee from Bell for his assistance with specimen manufacturing.

8. REFERENCES

1. Chambers, A.R., Earl, J.S., Squires, C.A., and Suhot, M.A. "The Effect of Voids on the Flexural Fatigue Performance of Unidirectional Carbon Fibre Composites Developed for Wind Turbine Applications" *Int. J. of Fatigue* 28(10) (2006): 1389-1398. https://doi.org/10.1016/j.ijfatigue.2006.02.033

2. Seon, G., Makeev, A., Nikishkov, Y., and Lee, E. "Effects of Defects on Interlaminar Tensile Fatigue Behavior of Carbon/Epoxy Composites" *Comp. Sci. & Tech.*, 89 (2013): 194-201. https://doi.org/10.1016/j.compscitech.2013.10.006

3. Lambert, J., Chambers, A.R., Sinclair, I., and Spearing, S.M. "3D Damage Characterisation and the Role of Voids in the Fatigue of Wind Turbine Blade Materials" *Comp. Sci. & Tech.* 72(2) (2012): 337-343. https://doi.org/10.1016/j.compscitech.2011.11.023

4. Seon, G., Makeev, A., Nikishkov, Y., and Fergusson, L. "Defect Formation in Contoured Composite Laminates During Vacuum Consolidation", Submitted to the Journal of the American Helicopter Society, 2019, Manuscript accepted with revision

5. Levy, A., Kratz, J. and Hubert, P. "Air Evacuation during Vacuum Bag Only Prepreg Processing of Honeycomb Sandwich Structures: In-Plane Air Extraction Prior to Cure" *Comp. Part A* 68 (2015): 365-376. https://doi.org/10.1016/j.compositesa.2014.10.013

6. Gangloff Jr, J.J., Simacek, P., Sinha, S. and Advani, S.G. "A Process Model for the Compaction and Saturation of Partially Impregnated Thermoset Prepreg Tapes" *Comp. Part A* 64 (2014): 234-244. https://doi.org/10.1016/j.compositesa.2014.05.010
7. Carrier, B. and Granet, S. "Numerical Modeling of Hydraulic Fracture Problem in Permeable Medium using Cohesive Zone Model" *Eng. Frac. Mech.* 79 (2012): 312-328. https://doi.org/10.1016/j.engfracmech.2011.11.012
8. Yao, Y., Liu, L. and Keer, L.M. "Pore Pressure Cohesive Zone Modeling of Hydraulic Fracture in Quasi-brittle Rocks" *Mech. of Mat.* 83 (2015): 17-29. https://doi.org/10.1016/j.mechmat.2014.12.010
9. Nguyen, V.P., Lian, H., Rabczuk, T. and Bordas, S., "Modelling Hydraulic Fractures in Porous Media using Flow Cohesive Interface Elements" *Eng. Geol.* 225 (2017): 68-82. https://doi.org/10.1016/j.enggeo.2017.04.010
10. Spencer, Anthony James Merrill, Ed. *Continuum Theory of the Mechanics of Fibre-Reinforced Composites*. Vol. 282. New York: Springer, 1984.
11. ABAQUS, v2016. User's Manual, ABAQUS Inc, Pawtucket, RI, USA, 2016
12. Turon, A., Camanho, P.P., Costa, J. and Dávila, C.G. "A Damage Model for the Simulation of Delamination In Advanced Composites under Variable-Mode Loading" *Mech. of Mat.* 38(11) (2006): 1072-1089. https://doi.org/10.1016/j.mechmat.2005.10.003
13. Bonet, J. and Burton, A.J. "A Simple Orthotropic, Transversely Isotropic Hyperelastic Constitutive Equation for Large Strain Computations" *Comp. Meth. in App. Mech. & Eng.* 162(1-4) (1998): 151-164. https://doi.org/10.1016/S0045-7825(97)00339-3